VTT Technical Research Centre of Finland

Simulation of Incompressible Viscous Flow Around a Tractor Thruster in Model and Full Scale

Sanchez Caja, Antonio; Ory, Emmanuel; Salminen, Esa; Pylkkänen, Jaakko; Siikonen, Timo

Published in:
8th International Conference on Numerical Ship Hydrodynamics

Published: 01/09/2003

Document Version
Publisher's final version

The 8th International Conference on Numerical Ship Hydrodynamics
September 22-25, 2003, Busan, Korea

Simulation of Incompressible Viscous Flow Around a Tractor Thruster in Model and Full Scale

Antonio Sánchez-Caja
VTT Industrial Systems, Finland
Email : Antonio.Sanchez@vtt.fi

Emmanuel Ory
Helsinki University of Technology
Email : ory@poseidon.hut.fi

Esa Salminen
Helsinki University of Technology
Email : Esa.Salminen@hut.fi

Jaakko Pylkkänen
VTT Industrial Systems, Finland
Email : Jaakko.Pylkkanen@vtt.fi

Timo Siikonen
Helsinki University of Technology
Email : Timo.Siikonen@hut.fi

ABSTRACT

The incompressible viscous flow around a podded propulsor of tractor type is simulated by solving the RANS equations with the k-ε turbulence model. The FINFLO solver developed at Helsinki University of Technology is used in the calculations. This paper presents the results of computations performed for a tractor thruster in model and full scale. Grids of up to 7.5 million cells were built for the hydrodynamic analysis. No wall functions were used. The sliding mesh technique was employed for modeling the rotating and stationary parts of the propulsor unit. Circumferential averaging over the sliding surface was applied in order to reduce the unsteady problem to steady state, and consequently decrease the CPU time. The calculated flow patterns are illustrated and the forces on the different components of the tractor unit are shown in model and full scale. The effect of insufficient grid size on the flow patterns is shown in model scale. Comparison of the calculated forces with experiments in model scale is also provided for one advance number. Good correlation is obtained in terms of total efficiency of the thruster. The predictions of the force coefficients for the different components are moderately good. The results give valuable information on scaling effects and guidance for the hydrodynamic design. This work was made within the European Union OPTIPOD project.

INTRODUCTION

Experiments in model scale have been long used as a basis for the extrapolation of propeller performance to full scale. Sometimes scale effects are not easily predictable due to the different flow regimes that can be present on the propulsor surfaces in model and full scale. This is the case of model tests for complex propulsion units in which passive components such as pods or ducts may experience areas of laminar flow whereas the flow over the propeller blades may be partially or totally turbulent. On the other hand the flow over the actual propulsor in full scale is usually completely turbulent and can display different extents of flow separation. This dissimilarity in flow regime is responsible in some particular cases for the lack of accuracy in the extrapolation of forces and cavitation behavior to full-scale. For the case of podded propulsors scale effects can be as significant as to decrease the full scale resistance coefficient of the housing to about 50-60 percent of the model measurements. Large propeller-wash and flow-separation phenomena are responsible for such differences, which is indicative of the need to develop more accurate extrapolation methods.

During the last decade numerical methods of RANS equation analysis have been increasingly applied to the prediction of scale effects. They have been found to provide valuable information on the quality of the flow both in model and full scale, and can be used in combination with model tests (Holtrop, 2001), or independently (Stanier, 1998), to quantify certain scale effects. Recently, the flow over a pod propulsor has been investigated in model and full scale (Lobachev et al., 2001) using an actuator disk model and a grid of 0.6 million cells. The propeller action was not scaled, i. e. the full scale thrust and torque coefficients were assumed equal to their model scale values.

Last year VTT Industrial Systems (VTT) and Helsinki University of Technology (HUT) investigated numerically the performance of a medium-speed podded propulsor unit using the FINFLO RANS solver. Rolls-Royce AB provided a test geometry

consisting of the housing and propeller data. This paper deals with the CFD analysis of the viscous flow around the propulsor in axially directed flow in model and full scale. A sliding mesh technique with circumferential averaging of flow quantities was employed for modeling the rotating and stationary parts of the propulsion unit. This technique allows to include the actual propeller geometry in the calculations with no need to make simplifications of actuator disk type for modeling the propeller action. At the same time the computational time is kept within reasonable limits. The initial grid for the flow simulation consists of 0.9 million cells, a size comparable to that presented in Sánchez-Caja et al. (1999). In this reference more emphasis was placed on modeling the propeller blades than the housing. This resulted in relatively higher concentration of cells over the propeller blades. As this grid size was found insufficient to accurately model the force coefficients over the entire thruster, it was decided to build a second grid of about 7.5 million cells for the present study. For the sake of completeness the single propeller without the housing has been numerically analyzed also in open water both in model and full scale and compared with model scale experiments.

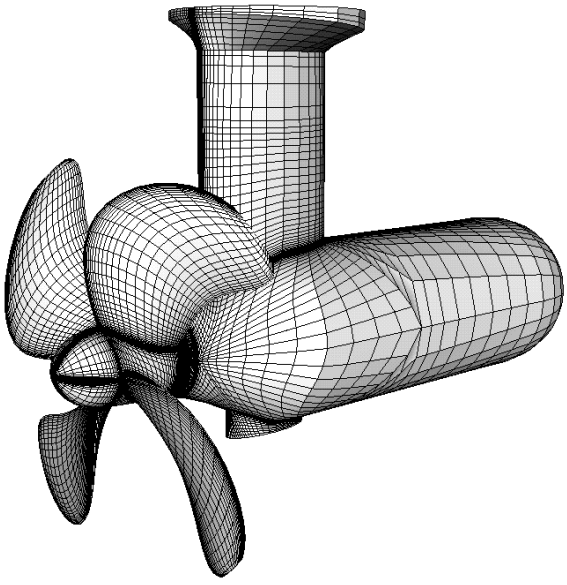

Figure 1. Grid on the podded propulsor surfaces. Initial grid (0.9 million cell grid).

NUMERICAL METHOD

FINFLO is a multiblock cell-centered finite-volume computer code with sliding mesh, moving-grid and free-surface capabilities. The flow simulation in FINFLO is based on the solution of the RANS equations by the pseudo-compressibility method combined with a sliding mesh technique. In this paper the concept of sliding mesh is used in a broad sense. Circumferential time averaging is applied to the sliding surface in order to reduce the unsteady problem to steady state, and consequently decrease the CPU time. FINFLO solves the RANS equations by a finite volume method. The solution is based on approximately factorized time-integration with local time-stepping. The code uses either Roe's flux-difference splitting or Van Leer's flux-vector splitting. A multigrid method is used for the acceleration of convergence. Solutions in coarse grid levels are used as starting point for the calculation in order to accelerate convergence. A detailed description of the numerical method including discretization of the governing equations, solution algorithm, etc. can be found in Sanchez-Caja et al. (1999 and 2000). Chien's low Reynolds number k-ε model has been used in the calculation.

SIMULATION IN MODEL SCALE

Geometry and Mesh

The podded propulsor is composed of a tractor propeller and a housing, which in turn includes a pod, a strut and a lower fin of short span.

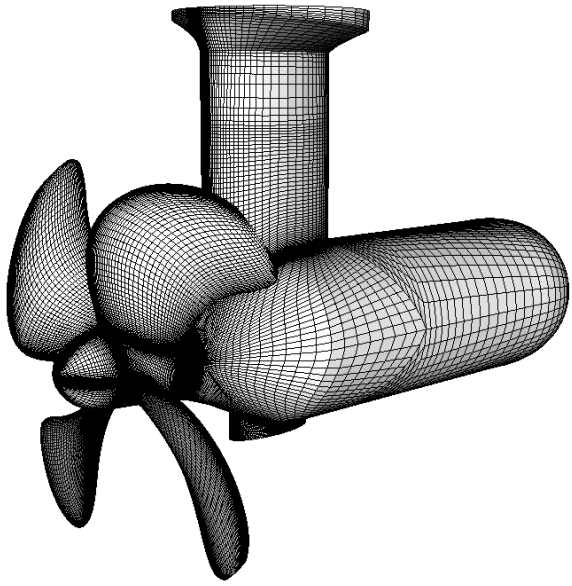

Figure 2. Grid on the podded propulsor surfaces. Fine grid (7.5 million cell grid).

The pod is a surface of revolution with a blunt downstream edge. The strut consists of a bi-symmetric profile of constant section extending vertically from the pod and a circular block for the connection to the ship hull. The fin is located at the same axial position of the strut underneath the pod.

The propeller is a four-bladed right-handed pro-

peller of 0.236 m diameter with moderate skew, with an expanded area ratio of 0.569. The onset flow for the calculations was 1.768 m/s and the rate of revolutions 12 rps, which corresponds to an advance number of 0.624. The hub diameter ratio is 0.179.

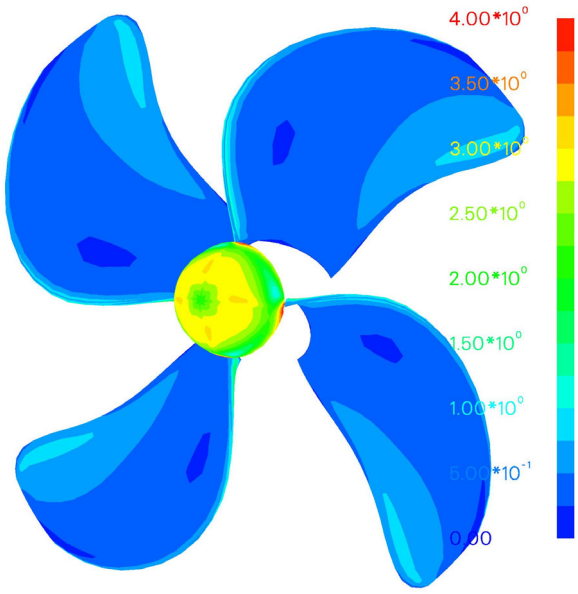

Figure 3. Distribution of y^+ over the propeller blades. Initial grid.

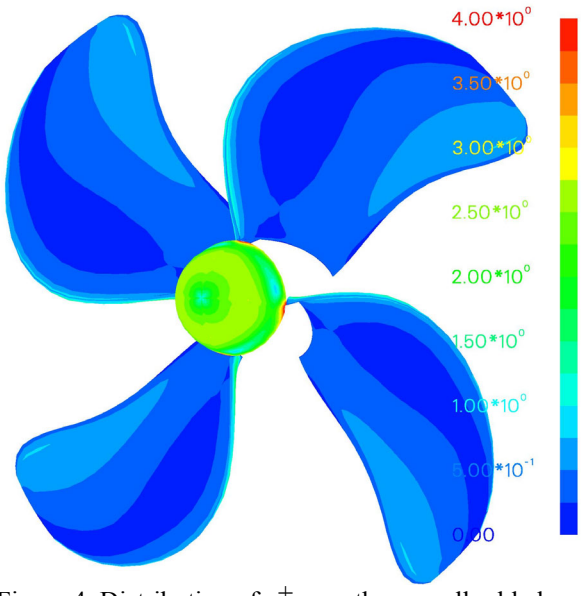

Figure 4. Distribution of y^+ over the propeller blades. Fine grid.

The initial grid for the podded propulsor calculation consists of about 0.9 million cells. Grids of such size were found to give useful qualitative information on the flow pattern around podded propulsors (Sánchez-Caja et al., 1999). However, such grids are clearly far from those required for a mathematically converged solution when no wall functions are used. For this reason a grid of about 7.5 million cells (1st grid level) was later built in order to obtain a better modeling of the flow. The blocks of this grid have double number of cells in each grid direction.

The grid used in the calculations is composed of 18 blocks. The number of blocks and cells per block was selected in order to evenly distribute the computational load between several processors. The grid topology was of O type around the strut and fin, and of H type around the propeller blades. In many respects such as location of grid boundaries, selected stretchings, etc, the grid was similar to those presented in Sánchez-Caja et al. (1999 and 2000), the main differences being confined to the fin and strut topology. Special emphasis was put on modeling the propeller blades and the part of the strut washed by the propeller wake.

The computational mesh on the strut-pod-propeller surfaces is shown for the initial grid in Figure 1 and for the fine grid in Figure 2. In the pictures only the surfaces used in the calculation of the thrust, drag forces and torque are displayed. The strut is extended above the area shown in the figures and ends in a short dummy streamlined body, but this part is not used for calculating the drag forces.

The y^+ values were found after computations close to unity over most of the surface being somewhat higher for the strut and hub than for the propeller blades. Figure 3 and 4 show the y^+ values over the propeller blade and hub cap for the initial grid and the fine grid, respectively.

A grid for the propeller alone with a conventional shaft was also built for a reference open water calculation. The grid has 1.05 million cells and only models the computational space between two blades benefiting from the periodicity of the solution. The accuracy of the propeller representation was the same as that of the 7.5 million cells for the podded propulsor.

Boundary Conditions

The boundary conditions were as follows. The upstream cap of the hub and blade surfaces of the propeller are rotating solid walls with boundary conditions enforcing the velocity field to match the propeller rotational speed. The velocities at the strut fin and pod surfaces are set to zero in order to satisfy the non-slip boundary condition. Because of CPU time considerations the calculations are based on a steady-state approach in which the flow is circumferentially averaged through a sliding surface located between

the propeller and the strut. For the single propeller calculation the lateral surfaces adjacent to the propeller blades have cyclic or periodic boundary conditions. At the computational infinity the boundary conditions are inspired from traditional propeller momentum theory, i.e. uniform flow is applied to the inlet and peripherical surfaces and the streamwise gradients of the flow variables as well as the pressure difference are set to zero at the outlet.

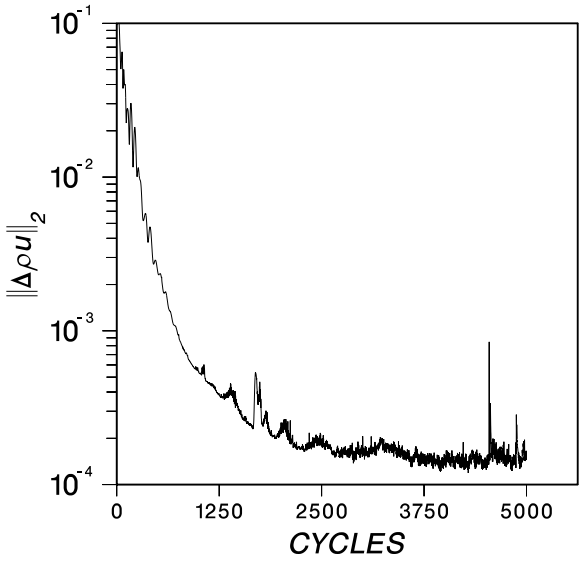

Figure 5. Convergence history of the x-momentum residuals. Coarse grid level of the initial grid.

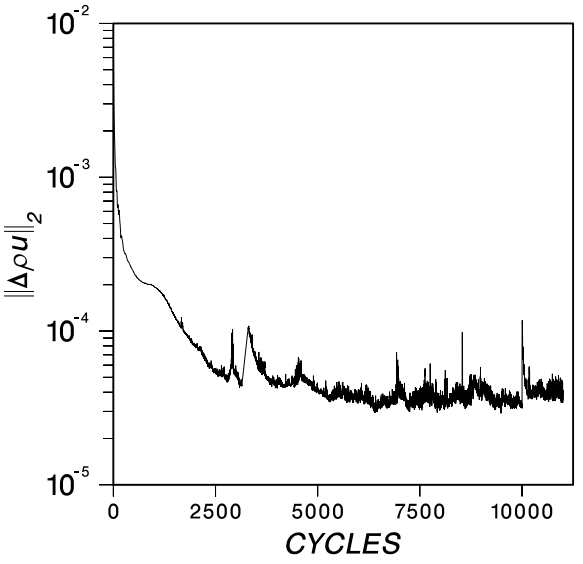

Figure 6. Convergence history of the x-momentum residuals. Fine grid level of the initial grid.

Convergence

The computations were performed on an SGI Origin 2000 machine. From 4 to 8 processors were used depending mainly on the grid size and processor availability. A satisfactory convergence was obtained with a Courant number of 0.5 using two multigrid levels. The convergence histories of x-momentum residuals are shown for a coarse grid level of the initial grid in Figure 5, and for the fine grid level of the same grid in Figure 6. As the computation for the fine grid level started from the values of the coarse one, the drop in orders of magnitude is smaller in Figure 6. The convergence of the overall drag coefficient is presented in Figure 7 as percentages of the final value. After 3000 iterations, the drag converged within 1 percent.

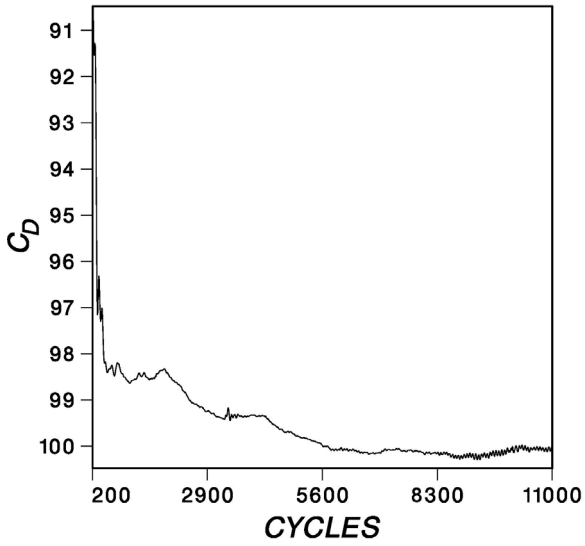

Figure 7. Convergence history of the overall drag coefficient. Fine grid level of the initial (coarse) grid.

Forces and Pressures

Experiments were made in two different test facilities. The first one was a towing tank and the second a cavitation tunnel. Large discrepancies were found in the experimental efficiency and thrust and torque levels between the two of them: 11 percent in thrust and 17 percent in torque coefficient. The Reynolds number was 0.4 million in the towing tank experiments and 1.15 million in the cavitation tunnel. Even though Reynolds number effects can cause differences in measurements, so large discrepancies were not expected. However, large differences have been found also by others (20th ITTC, Fig. 7.1). Tables Ia and Ib show the differences in percentages between calculations and experiments for the single propeller in uniform flow. They refer respectively to measurements in towing tank and cavitation tunnel. The computed thrust for the first grid level (fine grid) seems to correlate well with the measurements in the cavitation tunnel whereas the efficiency is closer to the values obtained in the towing tank. The computed torque is midway between those obtained in the two

facilities. The calculations were made for the towing tank flow conditions. The fact that the calculated torque and thrust levels are somehow shifted towards the cavitation tunnel measurements may mean that the turbulent regime was more developed in the calculations than in the towing tank experiments.

Table Ia. Propeller alone in uniform flow. Differences from measurements in towing tank.

%	2nd level	1st level
Kt	-16.0	-13.7
Kq	-4.6	-8.7
η	-11.3	-4.5

Table Ib. Propeller alone in uniform flow. Differences from measurements in cavitation tunnel.

%	2nd level	1st level
Kt	-5.2	-2.5
Kq	+11.7	+8.5
η	-16.1	-10.0

Note that in the tables the efficiency estimates in the second (coarse) grid level are more pessimistic than in the first one due to the small size of the grid: the efficiency is always underestimated with coarse grids, i.e. the torque overestimated relative to the thrust. Even though the grid used in this calculation is 30 percent smaller than that used in Sánchez-Caja et al., (1998 and 1999) and the geometry is also more complicated (skewed blades versus simple non-skewed blades of constant pitch), the main reason of the discrepancy in efficiency prediction is believed not to be the grid size. A finer grid would most probably slightly improve the prediction of efficiency. However, the thrust and torque levels presumably would not according to the tendency shown in Table Ia when moving from the coarse to the fine grid level. The main reason for the differences is believed to be in the deficiencies of the turbulence model for capturing a more complex flow over the skewed blades. In fact, for simple geometries at relatively high Reynolds number as those reported in the references above and also in Olsen (2001) the k-ε turbulence model seems to provide good estimates of performance coefficients. As the geometry becomes more complicated, for instance the thick blades in Pylkkänen et al. (1998), and especially the skewed blades presented here, the differences with experiments become larger. In particular the different extent of laminar flow in the tests relative to computations may partially explain such differences. In this connection Bazilevski (2001) has reported flow visualizations on conventional propeller models that show laminar boundary layer on both pressure and suction sides for Reynolds numbers similar to those presented in this work. The present tests were performed at a Reynolds' number of 0.4 million, without roughening on the blades, which might mean lower viscous forces in laminar regions in the absence of separation. In any case further study is needed to clarify the issue.

Table II. Podded propulsor unit in uniform flow. Differences from measurements in towing tank.

%	2nd level	1st level
Kt-unit	-17.1	-13.7
Kq	-4.6	-11.4
η-unit	-15.1	+1.8

Table II shows a remarkable improvement in the prediction of the total efficiency for the complete unit when passing from the second to the first grid level. The underestimation of drag in the non-rotating parts compensates the underestimation of thrust in the propeller blades, resulting in an improvement of the efficiency prediction. The presence of turbulent stimulators on the pod and strut during the tests can be partly responsible for the former underestimation as such stimulators tend to amplify drag forces. On the other hand the leading edges of the propeller blades were not artificially roughened, which may partially explain the underestimation of blade thrust in the computations.

Table III. Contributions of the different parts of the podded propulsor to the thrust. Model scale.

	2nd level	1st level
propeller blades	131.9	119.7
pod	-16.5	-10.1
lower fin	-0.6	-0.5
strut profile	-12.5	-7.7
strut circular block	-2.3	-1.4
Total	100.0	100.0
blades + rotating hub	131.5	119.3
non-rotating parts	-31.5	-19.3
Total	100.0	100.0

Table III shows the splitting of the forces for the different parts of propulsor unit. The total thrust of the unit is represented by +100%. The coarse grid seems to amplify both drag and thrusting forces relative to

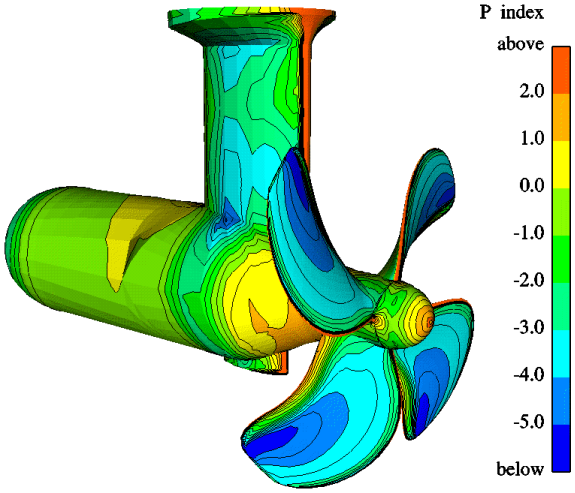

Figure 8. Pressure distribution on the suction (starboard) side of the podded propulsor. Initial grid.

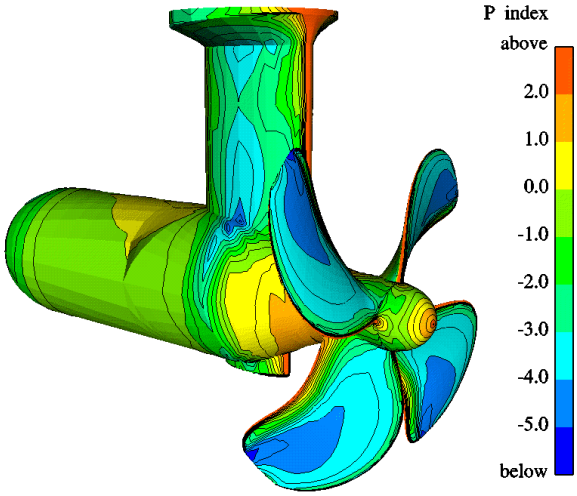

Figure 11. Pressure distribution on the suction (starboard) side of the podded propulsor. Fine grid.

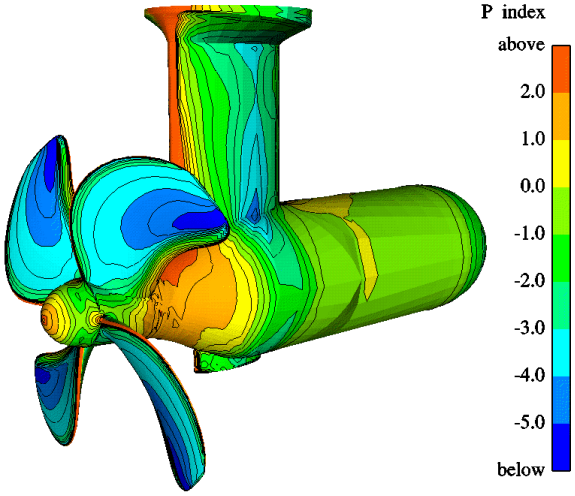

Figure 9. Pressure distribution on the pressure (port) side of the podded propulsor. Initial grid.

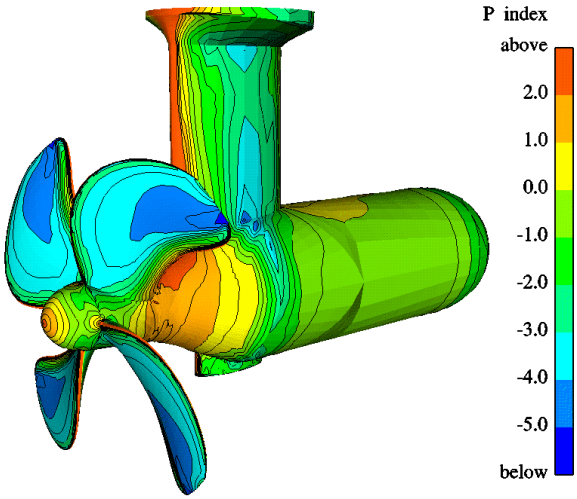

Figure 12. Pressure distribution on the pressure (port) side of the podded propulsor. Fine grid.

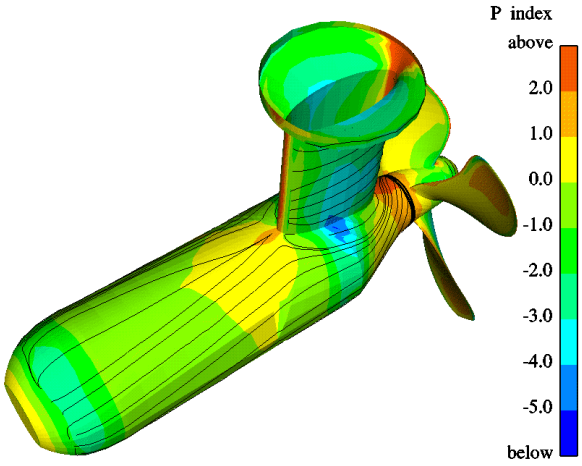

Figure 10. Streamlines on the suction (starboard) side of the podded propulsor. Back view. Initial grid.

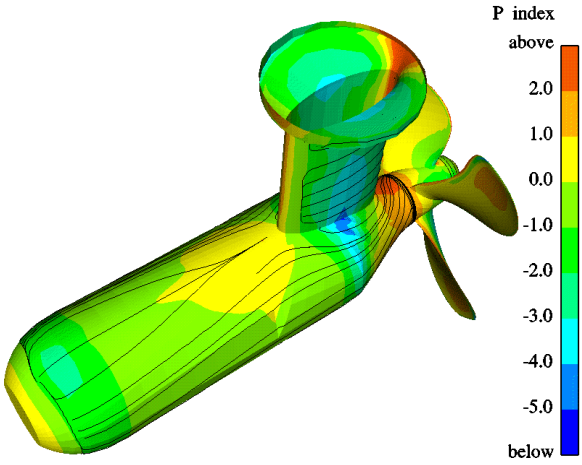

Figure 13. Streamlines on the suction (starboard) side of the podded propulsor. Back view. Fine grid.

the fine one. According to the predictions based on the fine grid the strut circular block decreases the thrusting force in more than 1 percent. In the vicinity of this block the boundary conditions have not been properly set since the hull of the ship has not been modeled. If the hull had been modeled, the flow would have been more 'two-dimensional' and the local velocities and frictional forces would have been somewhat higher. The contribution of the lower fin to the drag forces is about 0.5 percent.

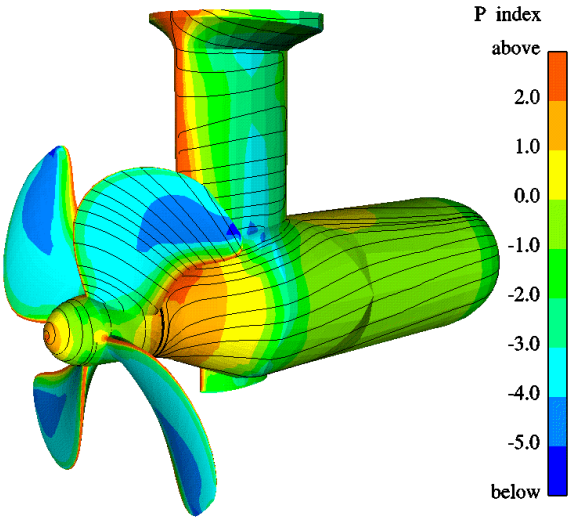

Figure 14. Streamlines on the pressure (port) side of the podded propulsor. Fine grid.

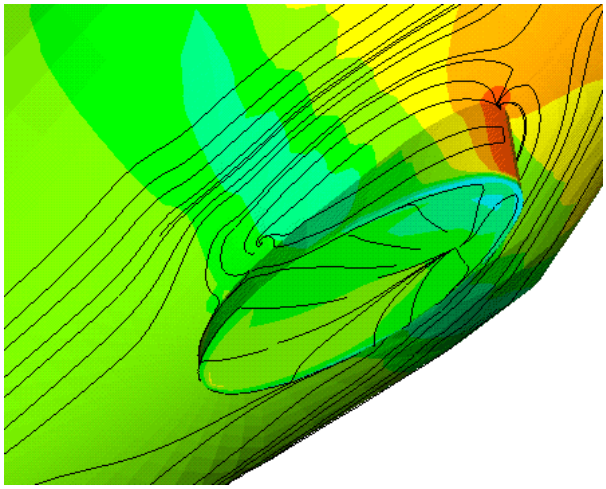

Figure 15. Streamlines on the starboard side of the bottom fin. Fine grid.

Flow analysis

Figures 8 and 9 show for the initial grid a general view of the pressure distribution on the suction (starboard) and pressure (port) side of the podded propulsor, respectively. The pressures are given as a nondimensional pressure index. One sub-contour is visible inside each color level. The lowest pressure appears at the propeller tips. A small low-pressure area is seen at the root of the strut at the axial location of maximum thickness within the propeller wake. Figure 10 shows streamlines on the pod and strut surfaces. Figures 11, 12 and 13 are the corresponding figures for the fine grid. The main difference that can be found for the fine grid calculation is the reduction of the low pressure area at the tip of the blade. Flow separation at the downstream blunt end of the pod and at the strut trailing edge is better captured by the fine grid.

Throughout the paper the results of the fine grid computation have been transferred to the initial grid for simplifying the data processing. For this reason the accuracy of pod geometry in the pictures is the same for the initial and fine grid, even though they contain results from computations with larger number of cells.

Figure 14 shows a front view of streamlines on the port side of the podded propulsor. The streamlines run smoothly over the propeller blade.

Figure 15 illustrates the high three-dimensionality of the flow on the bottom fin, with areas of flow separation on the lower surface and on the trailing edge of the fin. Notice that the pressure and suction sides of the fin are reversed relative to those of the strut due to the direction of the flow induced by the propeller rotation.

SIMULATION IN FULL SCALE

Geometry, Mesh and Boundary Conditions

For the full scale simulation the model scale grid was modified in order to set y^+ close to unity. The surface grids on the thruster surface were almost the same. Only the stretching in directions perpendicular to the solid surfaces was significantly modified. Therefore Figures 1 and 2 represent also the grid of the full scale calculation. The diameter at full scale was 3.55 m. Figure 16 shows y^+ values of about 3 over the propeller blade and hub cap for the fine grid. The boundary conditions were the same as those in the model scale calculation.

Convergence

The convergence histories of x-momentum residuals are shown for a fine grid level of the fine grid in Figures 17. As the computation in the fine grid level started from the values of the coarse one, the drop in orders of magnitude is similar to that in Figure 6. The convergence of overall drag coefficients is presented in Figure 18 as percentages of the final value.

Forces and Pressures

Table IV shows a comparison of performance coefficients between model and full scale calculations.

The full scale values are referred to the model scale ones (100). In full scale the thrust coefficient increases about 9 percent and the torque coefficient about 1 percent, which results in an increase of efficiency of about 8 percent. Table V shows a breakdown of non-dimensional force coefficients both in model and full scale. The values are relative to the non-dimensional total thrust of the thruster unit in model scale.

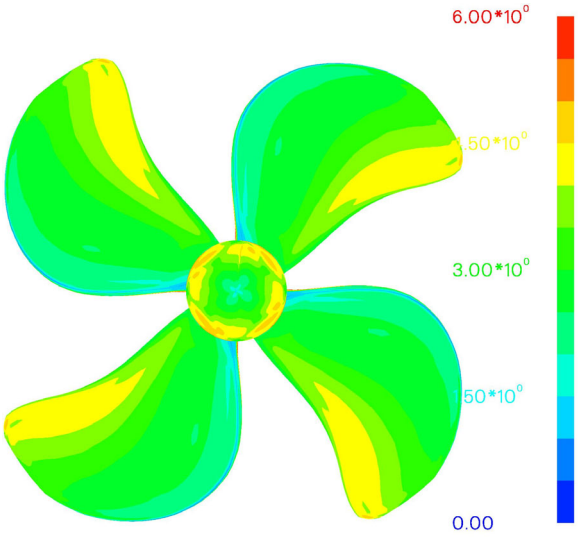

Figure 16. Distribution of y^+ over the propeller blades. Fine grid. Full scale calculation.

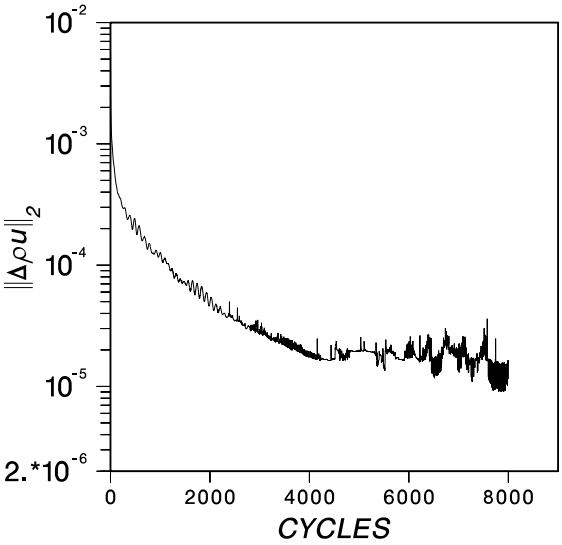

Figure 17. Convergence history of the x-momentum residuals. Fine grid level of the fine grid. Full scale.

The increase of thrusting force on the propeller blades and the decrease of drag on the strut for the full scale calculation are significant. The pod resistance does not noticeably decrease at full scale. It seems that the small reduction of pod resistance is probably due to the blunt downstream edge. The relative reduction of flow detachment (and consequently of drag) in full scale cannot be as large for the pod as for the strut. The truncated shape of the pod edge forces a premature detachment, which did not occur at the strut trailing edge. The total reduction of drag for the non-rotating parts is 14 percent.

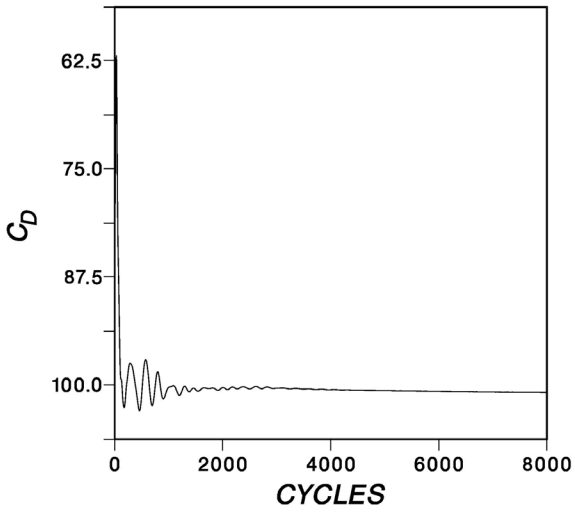

Figure 18. Convergence history of the overall drag coefficient. Fine grid level of the fine grid. Full scale.

Table IV. Comparison of performance coefficients for the tractor thruster. Model versus full scale.

scale	full	model
Kt-unit	108.8	100
Kq	100.9	100
η-unit	107.8	100

Table V. Comparison of force coefficients over the components of the thruster. Model versus full scale.

scale	full	model
propeller blades	125.67	119.65
pod	-9.92	-10.09
lower fin	-0.45	-0.45
strut profile	-5.93	-7.77
strut circular block	-0.59	-1.35
Total	108.78	100.0
blades + rotating hub	125.36	119.24
non-rotating parts	-16.58	-19.24
Total	108.78	100.0

Table VI shows in percentages the relative contribution of the frictional forces to the total forces (fric-

tional + pressure) for each of the components in the thruster. For instance, for the strut profile in full scale the frictional resistance is 14 percent of the total one and consequently the pressure resistance is 86 percent. The relative small and negative percentages for the propeller blades (or rotating parts) are due to the fact that the propeller blades are providing not only drag as the other components do but also a large pressure-based thrust (negative drag). Applying the percentages of Table VI to those in Table V the viscous and pressure components of the resistance can be obtained in absolute terms relative to the thrust of the propulsion unit in model scale. They are shown in Table VII.

Table VI. Frictional resistance as relative percentage of the total resistance of each component.

scale	full	model
propeller blades	-1.3	-1.7
pod	13.3	22.0
lower fin	12.2	14.3
strut profile	14.0	15.6
strut circular block	12.3	8.8
rotating parts	-1.4	-1.8
stationary parts	13.2	18.9

Table VII. Frictional and pressure resistance as absolute percentage of the unit thrust.

scale	full		model	
%	Cf	Cp	Cf	Cp
propeller blades	-1.67	127.35	-2.02	121.67
pod	-1.32	-8.60	-2.22	-7.87
lower fin	-0.05	-0.39	-0.06	-0.38
strut profile	-0.83	-5.10	-1.21	-6.56
strut circ. block	-0.07	-0.52	-0.12	-1.23
rotating parts	-1.76	127.13	-2.14	121.38
stationary parts	-2.18	-14.39	-3.50	-15.74

Moving from model to full scale the pod frictional resistance decreases considerably (Table VI and VII). However, the pressure resistance grows making the total resistance of the pod only slightly smaller in full scale (Table V). For the strut profile, both the pressure and frictional resistance decrease significantly in full scale (22 and 31 percent), which results in a total drag reduction of 24 percent. The reduction of pressure resistance in this case is connected to the development of a lifting force by the profile subject to oblique flow caused by the tangential components of the propeller-induced velocity. For the strut circular block, even though in relative terms the frictional resistance seems to grow (Table VI), in absolute terms (Table VII) the percentual reductions are even greater, 58 for the pressure, 42 for the frictional and 56 for the total resistance. For the propeller blades the frictional resistance decreases in 17 percent and the pressure thrust increases in about 5 percent. The lower fin is not much affected by the scale change.

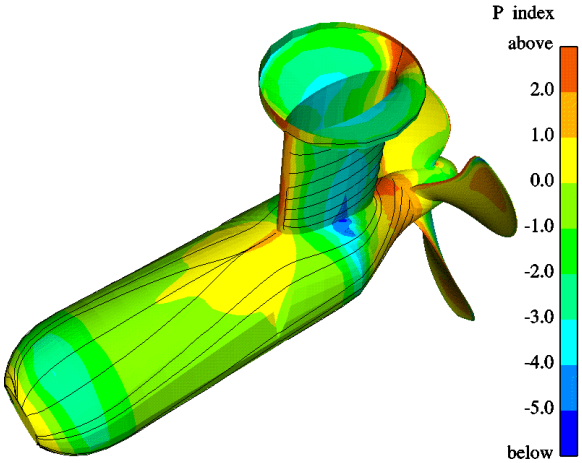

Figure 19. Streamlines on the suction (starboard) side of the podded propulsor. Fine grid. Full scale.

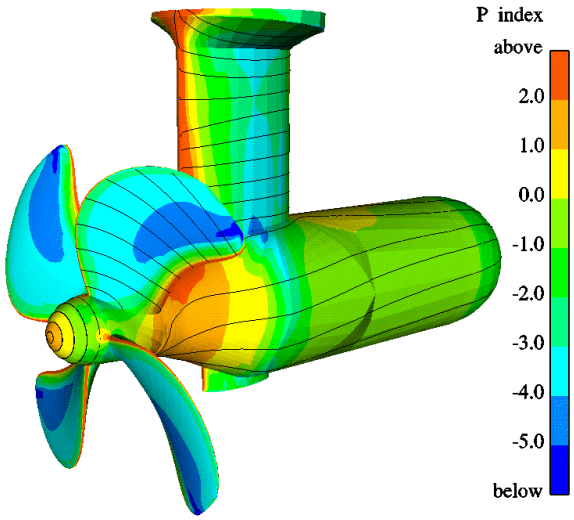

Figure 20. Streamlines on the pressure (port) side of the podded propulsor. Fine grid. Full scale.

For the sake of completeness the computation for the propeller alone , i.e. without the pod housing, was made in full scale also. Table VIII shows the propeller performance coefficients in full scale as percentages of its model scale values. The torque coefficient

increases in 1.1 percent and the blade thrust coefficient increases in 7.9 percent. The changes experienced by the propeller blades of the complete tractor thruster are. 0.9 percent increase in torque (Table IV) and 5 percent increase in blade thrust (=125.7/119.7, Table V). The corresponding increases of *blade* efficiency are 6.7 percent for the propeller alone and 4.1 percent for the tractor thruster. Interaction effects are believed to be partly responsible for such differences in scaling behavior, which affects mainly the scaling of thrust.

Table VIII. Comparison of performance coefficients for the propeller alone. Model versus full scale.

scale	full	model
Kt-blades	107.9	100
Kq	101.1	100
η-blades	106.7	100

Flow analysis

Figure 19 shows streamlines on the pod and strut surfaces for the fine grid in full scale. Figure 13 is the corresponding figure in model scale. It is apparent that the extent of flow separation at the downstream blunt end of the pod and at the strut trailing edge is smaller in full scale. This contributes to the reduction of drag forces on the strut and pod mentioned in the previous section.

Figure 20 shows a front view of streamlines on the port side of the podded propulsor. The streamlines run smoothly over the propeller blades as was the case in Figure 14. The extent of low pressure at the tip is slightly larger than that in model scale.

CONCLUSIONS

The incompressible viscous flow around a tractor thuster has been simulated both in model and full scale by solving the RANS equations with the k-ε turbulence model. Circumferential average of the flow variables was applied on a sliding surface located between propeller and strut.

From the standpoint of code verification, the effect of the grid size in the computed forces and flow patterns has been illustrated in model scale. Quantitatively coarse grids tend to overpredict forces and to underpredict efficiencies relative to fine grids. Qualitatively coarse grids tend to underpredict the extent of flow separation.

From the standpoint of code validation, large discrepancies between experiments performed in towing tank and cavitation tunnel make suspect the presence of partial laminar flow in the towing tank experiments. The task of predicting forces by the RANS solver becomes more difficult in mixed flow regimes.

For the propeller without pod housing, the calculated torque coefficient seems to be about the average of the values obtained in the two facilities. The thrust coefficient however is closer to the cavitation tunnel measurements (2 percent), and the efficiency to those of the towing tank (4.5 percent). For the podded propulsor unit the total efficiency measured in the towing tank is well captured with the 7.5 million cell grid (1.8 percent difference) and strongly underpredicted with the 0.9 million cell grid (15 percent). The levels of torque and thrust are underpredicted by more than 10 percent for the fine grid.

The computations have been made for the same thruster geometry in full scale. The forces on the different components of the tractor unit are shown and compared to model scale results. Large differences are found in the scaling of various passive components of the thruster, which is illustrative on why classical scaling laws used for conventional propellers are not adequate for complex propulsors. In particular the full scale resistance ranges between 44 to 100 percent of the model resistance for the different components. Reduction of pressure drag in the strut profile is interpreted as a generation of lifting force on the profile under propeller-induced oblique flow. The total resistance of the non-rotating components lift in full scale is reduced in 14 percent.

Calculated flow patterns in full scale have been illustrated and compared to those obtained in model scale. Flow detachment on the pod and strut surfaces is delayed in full scale.

The RANS analysis performed under this investigation was found useful to understand better from a hydrodynamic standpoint the complex interaction between the propeller and the passive components in a podded propulsor.

ACKNOWLEDGEMENTS

This work has been made within the European Union OPTIPOD project. The computing time was partly provided by the Center for Scientific Computing of Finland. The authors wish to thank the partners in the OPTIPOD project for allowing this publication. Special thanks are given to Rolls Royce for providing the geometry subject to investigation.

REFERENCES

Bazilevski, Y.S., "On the Propeller Blade Turbulization in Model Tests." Lavrentiev Lectures, St. Petersburg (Russia), 2001, pp. 201-206.

Holtrop, J. "Extrapolation of Propulsion Tests for Ships with Appendages and Complex Propulsors."

Marine Technology, Vol. 38, No. 3, July 2001, pp. 145-157.

Lobachev, M.P., Tchitcherine, I.A., "The Full Scale Estimation for Podded Propulsion System by RANS Method." Lavrentiev Lectures, St. Petersburg (Russia), June 19-21, 2001.

Olsen, Anders S., "Investigation of the Viscous Flow Around Two Model Propellers in Uniform Flow." Helsinki University of Technology, Laboratory of Applied Thermodynamics, Report 130, 2001.

Proceedings of the 20th International Towing Tank Conference. Report from the Propulsion Committee. Vol I. San Francisco (California), September 19-25 1993.

Proceedings of the 23rd International Towing Tank Conference. Report from the Propulsion Committee. Vol I. Venice (Italy), September 8-14, 2002.

Pylkkänen, J.V., Sánchez-Caja, A. "Numerical Calculation of Viscous Flow Around an Old Ice Breaker Propeller for a Wide Advance Number Range Using the FINFLO Navier-Stokes Solver." VTT Report VALB306, March 1998, 26 pages.

Sánchez-Caja, A., "DTRC Propeller 4119 Calculations at VTT," VTT Report VALB304. Presented at 22nd ITTC Propulsion Committee Propeller RANS/Panel Method Workshop, Grenoble, April 5-6, 1998.

Sánchez-Caja, A., Rautaheimo, P., Salminen, E., and Siikonen, T., "Computation of the Incompressible Viscous Flow around a Tractor Thruster Using a Sliding Mesh Technique," 7th International Conference in Numerical Ship Hydrodynamics, Nantes 1999.

Sánchez-Caja, A., Rautaheimo, P. and Siikonen, T., "Simulation of Incompressible Viscous Flow Around a Ducted Propeller Using a RANS Equation Solver," 23rd Symposium on Naval Hydrodynamics, Val de Reuil (France), 2000.

Stanier, M., "The Application of RANS code to Investigate Propeller Scale Effects." Proc. of 22nd ONR Symposium, Washington (USA), 1998, pp. 222-238.